JOURNAL OF MATERIALS SCIENCE 26 (1991) 6699–6705

Low temperature and strain rate dependence of fracture stress and fracture toughness on thin $Fe_{40}Ni_{40}B_{20}$ amorphous ribbon

V. OCELÍK*, V. Z. BENGUS, E. B. KOROLKOVA
Institute for Low Temperature Physics and Engineering, Ukr. SSR Academy of Sciences, Lenin Avenue 47, 310 164 Kharkov, USSR

K. CSACH, J. MIŠKUF
Institute of Experimental Physics, Slovak Academy of Sciences, Solovjevova 47, 040 01 Košice, Czechoslovakia

P. DUHAJ
Institute of Physics, Slovak Academy of Sciences, Dúbravská cesta 28, 842 28 Bratislava, Czechoslovakia

The fracture stress and the critical stress intensity factor of the $Fe_{40}Ni_{40}B_{20}$ amorphous metallic ribbons 20 μm thick were measured in the temperature range 4.2–300 K and at deformation rates from 3.3×10^{-6} to 1.25×10^{-3} m^{-1} with the aim to obtain more information on the condition for the onset and development of the inhomogeneous plastic deformation and fracture.

1. Introduction

Plastic deformation of metallic glasses (MG) at temperatures much lower than the glass transition temperature T_g is realized via inhomogeneous shear in narrow shear bands [1, 2]. Conditions of the shear bands creation and resulting MG failure during tensile test have been studied for a longer time. Numbers of papers was devoted to the study of the influence of temperature and/or deformation rate on the fracture stress [3–5] and the fracture toughness [6–8] of these materials.

In this paper we simultaneously observe the influence of both the temperature and the deformation rate on the two above mentioned mechanical characteristics of MG.

2. Experimental details and results

On $Fe_{40}Ni_{40}B_{20}$ samples with dimensions of $20 \times 10 \times 0.02$ mm^3 the fracture stress σ_{fr} and the fracture toughness K_c were measured at deformation rates $\dot{\varepsilon} = 3.3 \times 10^{-6}$, 1.3×10^{-5}, 1.25×10^{-4}, 1.25×10^{-3} s^{-1} and at temperatures T of 300 K (air), 77 K (liquid nitrogen) and 4.2 K (liquid helium). Metallic glass was prepared by planar flow casting method from the melt having a temperature of 1340 °C. Tensile tests were performed 18 months after the samples have been produced. Centrally located cracks necessary to determine the fracture toughness from the tensile test record [9] were prepared by the local hydrogenation of the sample resulting in temporary embrittlement [10], followed by bending until a sharp crack was formed. The fracture surfaces were observed by a scanning electron microscope TESLA BS 300, the crack length before and after sample failure was measured using an optical microscope.

2.1. Fracture toughness

The dependence of the fracture toughness on the temperature and on the deformation rate is shown in Fig. 1a and b where the mean value from five measurements is indicated together with 95% reliability bars. Results of the statistical evaluation of measured data, using the dispersion analysis method, confirmed the strong dependence of K_c on temperature for all applied deformation rates. On the contrary, the dependence of K_c on the deformation rate was statistically proved only at a temperature of 300 K.

The fracture surface just behind the *a priori* crack is schematically shown in Fig. 2. It consists of: (a) a chevron fracture region (except for some of T, $\dot{\varepsilon}$ combinations); and (b) an area of shear ductile failure characterized by the smooth part of the fracture surface and by the vein morphology with an apparent main vein. The distance of this main vein from the ribbon edge determines the displacement size in the shear band. Vector of displacement forms an angle of approximately 45° with the ribbon surface and also with the tensile stress direction. On the smooth part some steps (stairs), single or in groups, may be observed, which are caused by displacements in a number of not exactly parallel shear bands.

* *Permanent address*: Institute of Experimental Physics, Slovak Academy of Sciences, Solovjevova 47, 040 01 Košice, Czechoslovakia.

0022–2461/91 $03.00 + .12

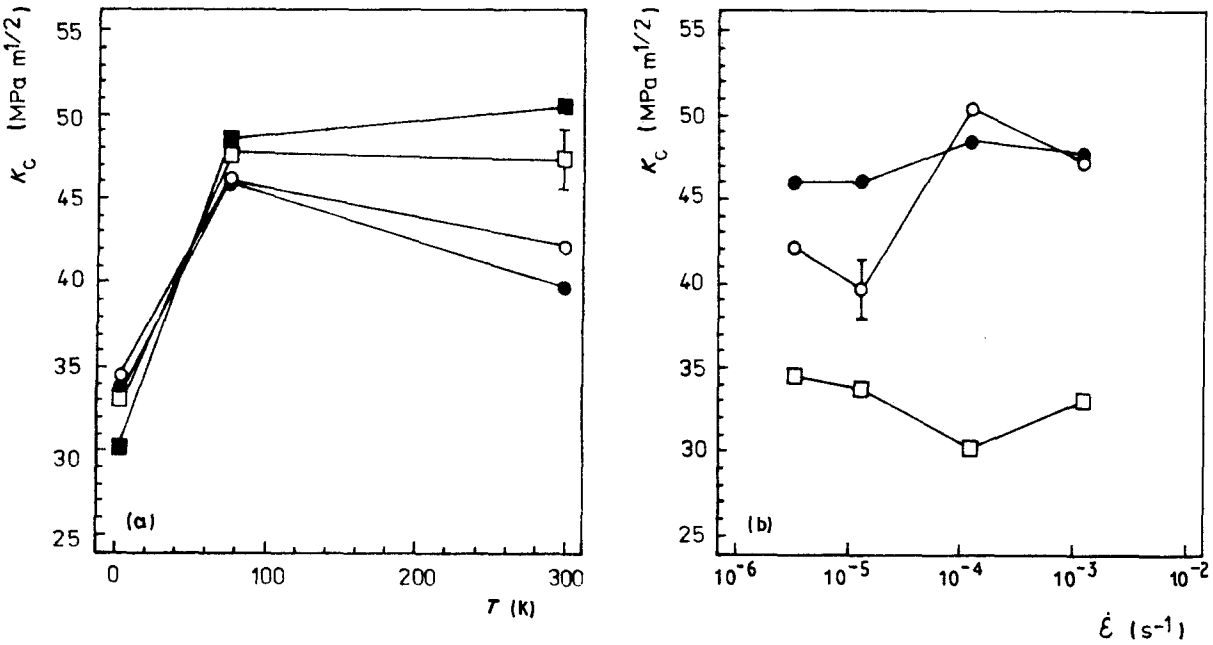

Figure 1 Fracture toughness dependence of $Fe_{40}Ni_{40}B_{20}$ MG: (a) on the temperature for various deformation rates: (○) 3.3×10^{-6}; (●) 1.3×10^{-5}; (■) 1.25×10^{-4}; (□) 1.25×10^{-3} s^{-1}; and (b) on the deformation rate for various temperatures: (○) 300; (●) 77; (□) 4.2 K.

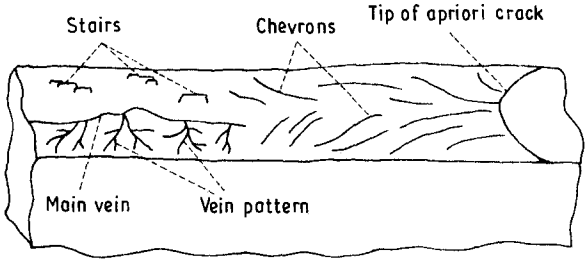

Figure 2 Schematic appearance of the fracture surface of a sample failed during K_c measurement, place just behind an *a priori* crack.

Fractographic observation of fracture surfaces near the root of an *a priori* crack on samples failed at different temperatures and deformation rates revealed following features: at 300 K (i) the chevron area is not present at all; (ii) for higher deformation rates (1.25×10^{-4} and 1.25×10^{-3} s^{-1}) the displacement value is almost equal to the width of the fracture surface, i.e. the main vein is near the edge of the fracture surface, while for lower deformation rates (3.3×10^{-6} and 1.3×10^{-5} m^{-1}) the displacement is lower than half of the fracture surface width; and (iii) steps on the fracture surface are apparent and are found on the whole smooth part of the fracture surface.

As an example, Fig. 3a shows the fracture surface of a sample failed at a deformation rate 1.25×10^{-3} s^{-1}, for which the value of $K_c = 45.3$ MPa m$^{1/2}$ was determined. At 77 K: (i) the chevron area is found on samples failed at higher deformation rates, usually in front of one of the crack tips, and is about 120 μm long; and (ii) a few steps are observable on the fracture surface. At 4.2 K: (i) the chevron area of the fracture surface is present for all deformation rates and is about 200 μm long; (ii) the displacement value at shear deformation has similar behaviour as for samples failed at 300 K; and (iii) no steps on the fracture surface were observed.

Fig. 3b shows part of the fracture surface, on which a ductile failure in the plane of maximum tensile stresses (chevron pattern) is changed into a ductile failure in the plane of maximum shear stresses (vein pattern), for sample failed at a deformation rate of 3.3×10^{-6} s^{-1} at 4.2 K, with the measured value of $K_c = 35.0$ MPa m$^{1/2}$. Crack propagated from right, distance of the shown area from the tip of an *a priori* crack is about 200 μm.

2.2. Fracture stress

Fig. 4a, b shows the dependence of the fracture stress on the temperature and on the deformation rate. Each of indicated values represents an average from 8–10 measurements and the range of 95% reliability is also shown. It may be seen, that the dependence of the fracture stress on the temperature is not so strong as that of K_c, and that the dependence of σ_{fr} on $\dot{\varepsilon}$ is more or less apparent only for the temperature of 4.2 K.

Evaluation of the fracture stress measurements revealed an interesting fact. All samples (8–10) which failed at given temperature T_i and at deformation rate $\dot{\varepsilon}_j$ could be divided into two groups distinguished by the macroscopic appearance of the fracture, see Fig. 5. In one group (fracture stress values for this group are indicated by the index "⊥") a failure macroscopically perpendicular to the tensile direction prevailed, in the other one (with fracture stress values indicated by "∠") the larger part of the sample cross-section macroscopically failed at an angle of 25–55° to the tensile axis. This distribution of samples into two groups corresponded also to observed values of σ_{fr} in both groups, where for every i–j pair the relation was valid:

$$\sigma_{fr\angle}(T_i, \dot{\varepsilon}_j) > \sigma_{fr\perp}(T_i, \dot{\varepsilon}_j) \quad (1)$$

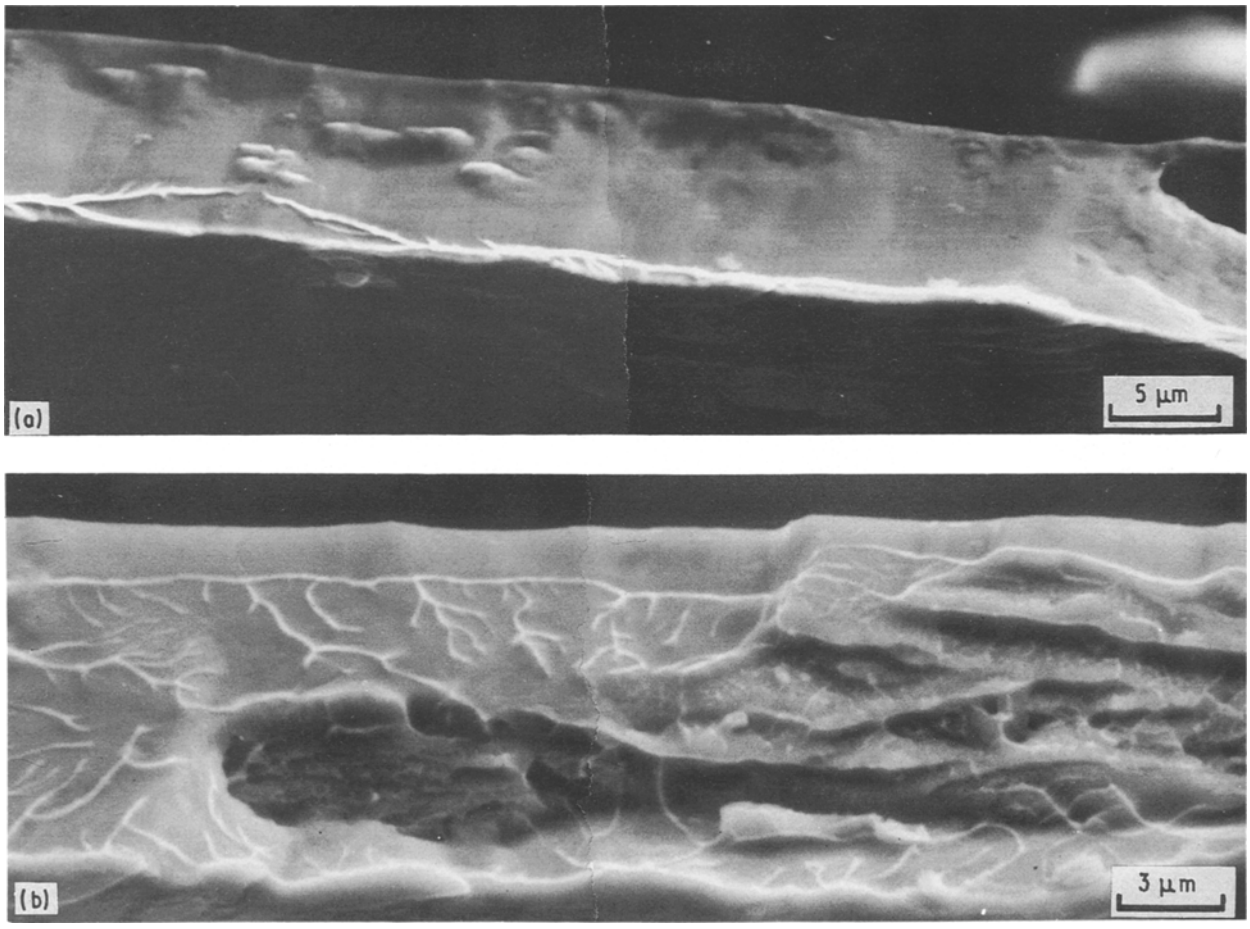

Figure 3 SEM of the fracture surface for a sample failed during K_c measurement: (a) temperature 300 K, deformation rate 1.25×10^{-3} s^{-1}; and (b) temperature 4.2 K, deformation rate 3.3×10^{-6} s^{-1}.

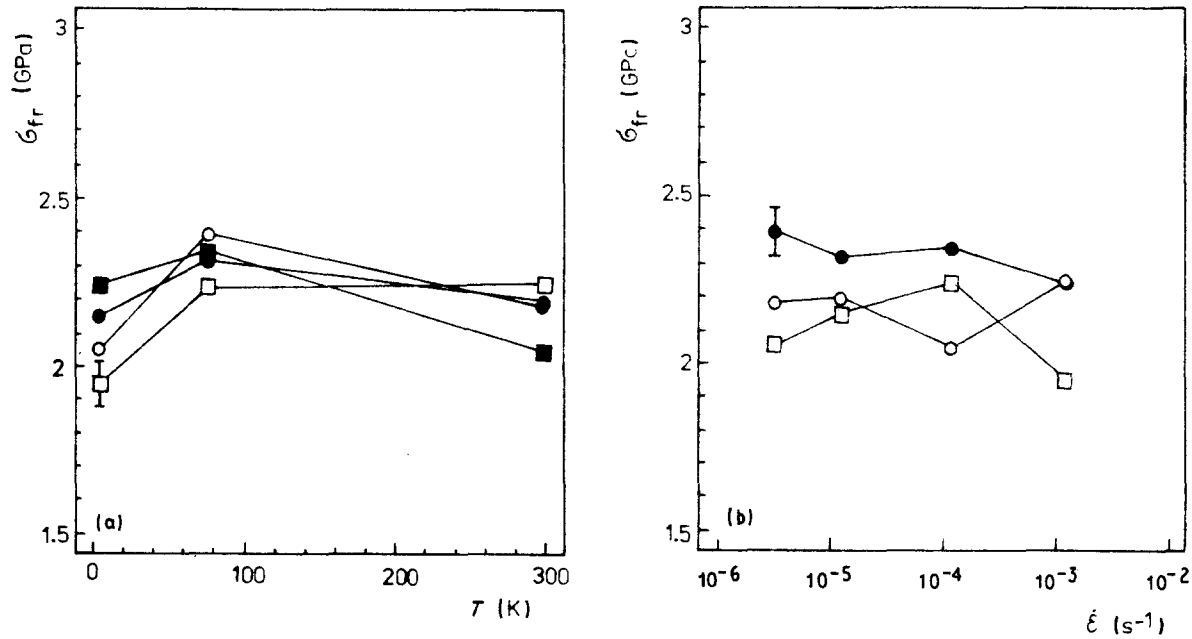

Figure 4 Fracture stress dependence of $Fe_{40}Ni_{40}B_{20}$ MG: (a) on the temperature for various deformation rates: (○) 3.3×10^{-6}; (●) 1.3×10^{-5}; (■) 1.25×10^{-4}; (□) 1.25×10^{-3} s^{-1}; and (b) on the deformation rate for various temperatures: (○) 300; (●) 77; (□) 4.2 K.

It was shown in [7, 11], that for the statistical distribution of the MG fracture stress the Weibull probability model may be successfully applied:

$$P_{fr}(\sigma) = 1 - \exp\left[- V\left(\frac{\sigma}{\sigma_0}\right)^m \right] \qquad (2)$$

where σ_0 is scaling parameter, m the Weibull modulus and V volume of tested sample. Our observations confirm this result, even when the influence of volume [11] was not checked. Fig. 6a shows the Weibull transformation of the empiric distribution function for the whole set of 102 samples. Fig. 6b shows this

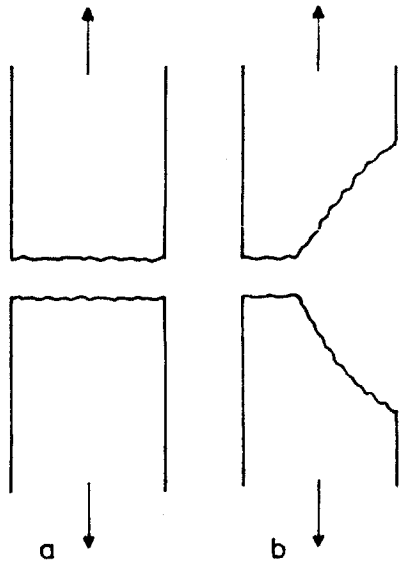

Figure 5 Two macroscopically different modes of failure observed at the tensile test: (a) perpendicular; and (b) oblique fracture.

transformation separately for particular temperatures. Temperature decrease is manifested by decrease of the Weibull modulus from 10 at 300 K to 9.0 at 77 K and 5.6 at 4.2 K. In Fig. 6c the Weibull transformation is shown separately for the two macroscopically observed failure modes.

From the above discussion it seems necessary to study the $\sigma_{fr}(T, \dot{\varepsilon})$ behaviour separately for each mode of the macroscopic failure, as shown in Fig. 5. The two dependences for two distinctive failure modes are in Fig. 7a, b. It is evident, that the dependences $\sigma_{fr}(T)$, $\sigma_{fr}(\dot{\varepsilon})$ may be considered as qualitatively the same. However, it should be taken into account, that points in these dependences represent an average value $\bar{\sigma}_{fr}$ from a number of measurement and they do not have the same statistical weight, because percentage of samples failed by the different failure mode varied in dependence on temperature and deformation rate, as shown in Table I.

It is seen that with decreasing temperature the relative participation of the perpendicular fracture increases. Monotonic dependence of the perpendicular fracture percentage on $\dot{\varepsilon}$ may be observed only at 4.2 K, where this percentage increases with increasing deformation rate.

TABLE I Percentage of samples failed through the macroscopically perpendicular fracture

T(K)/$\dot{\varepsilon}$(s^{-1})	3.3×10^{-6}	1.3×10^{-5}	1.25×10^{-4}	1.25×10^{-3}
300	37.5	25.0	50.0	25.0
77	55.6	62.5	37.5	62.5
4.2	50.0	62.5	70.0	70.0

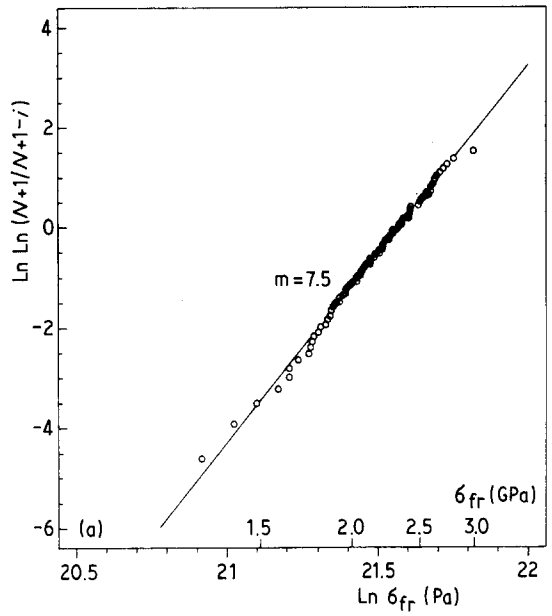

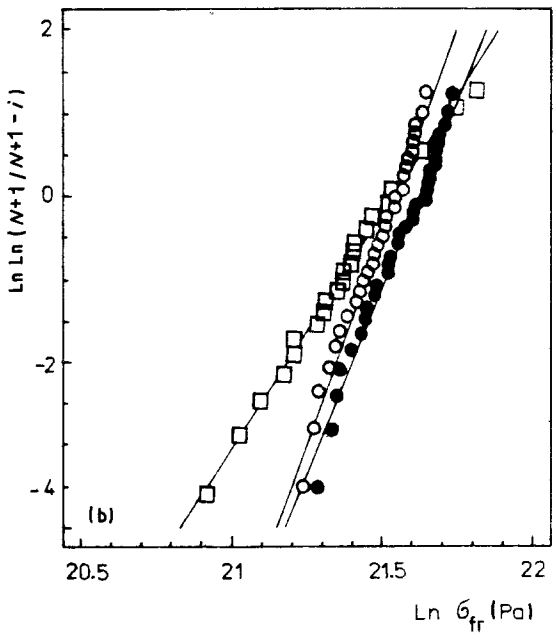

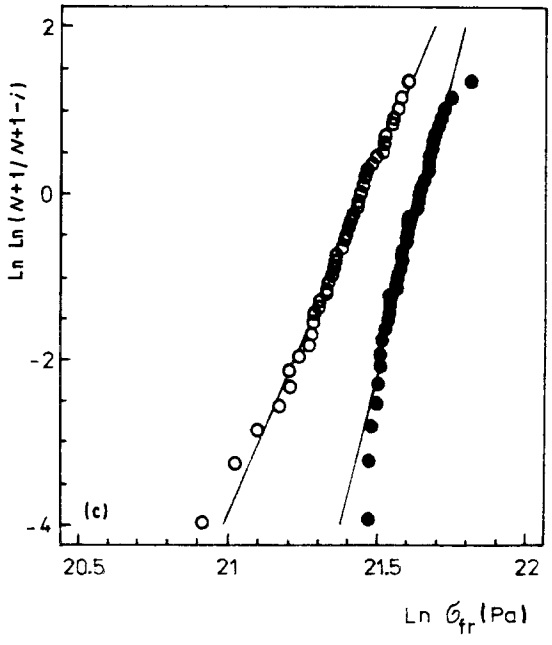

Figure 6 Weibull transformation of the empiric distribution function of the fracture stress for $Fe_{40}Ni_{40}B_{20}$ MG: (a) for all temperatures and deformation rates; (b) separately for temperatures: (○) 300; (●) 77; (□) 4.2 K; and (c) separately for two macroscopically different failure modes: (○) perpendicular fracture and (●) oblique fracture.

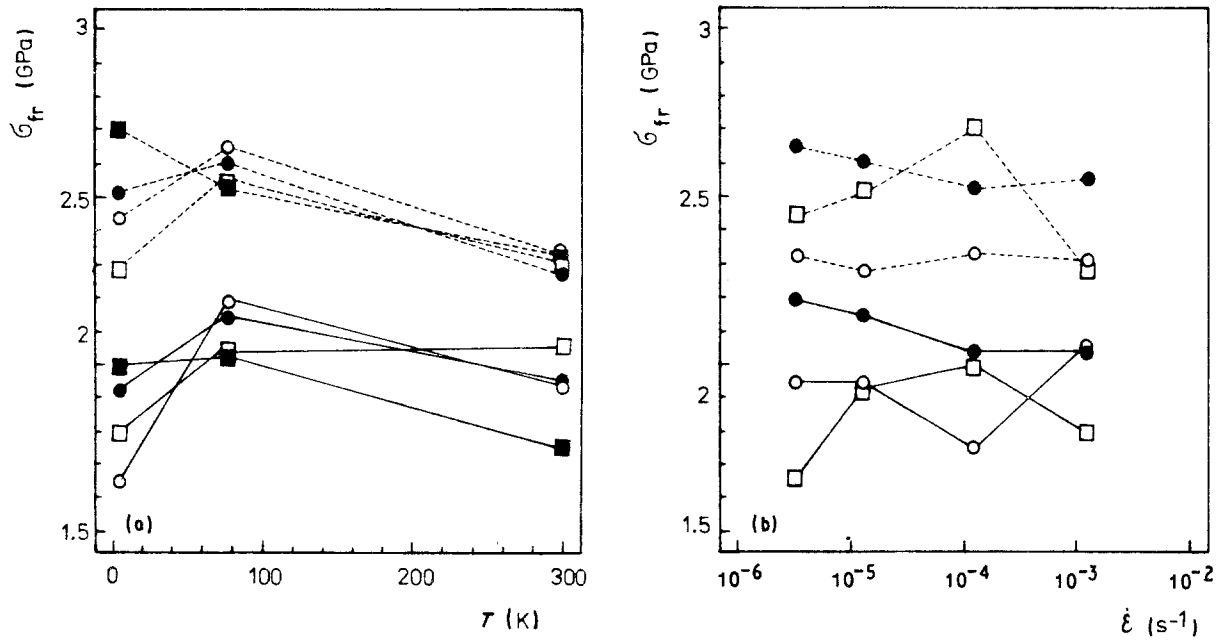

Figure 7 Dependence of (——) $\sigma_{fr\perp}$ and (– – –) $\sigma_{fr\angle}$ (see text): (a) on the temperature for various deformation rates: (○) 3.3×10^{-6}; (●) 1.3×10^{-5}; (■) 1.25×10^{-4}; (□) 1.25×10^{-3} s^{-1} and (b) on the deformation rate for various temperatures: (○) 300; (●) 77; (□) 4.2 K.

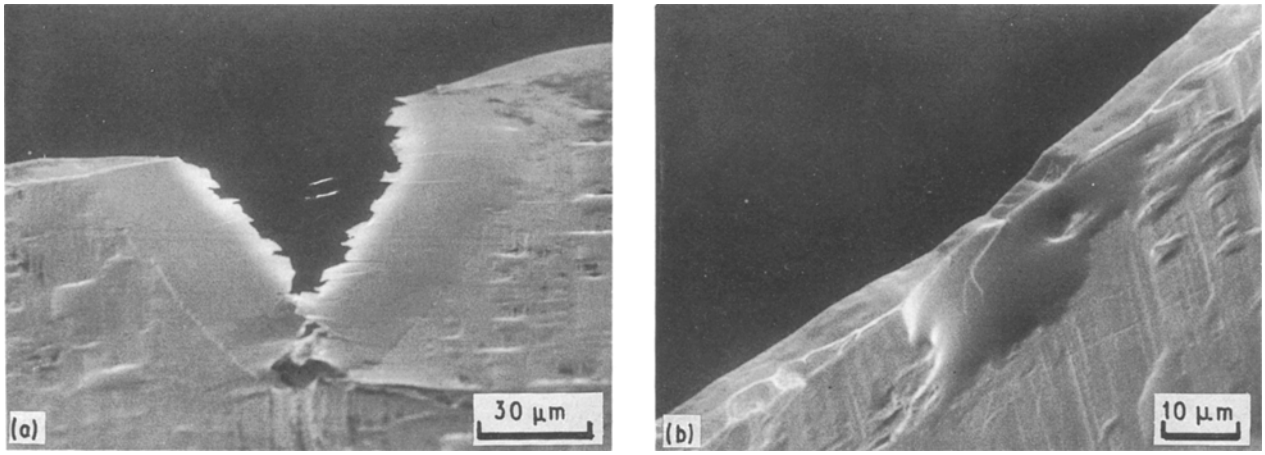

Figure 8 Initiation sites of the $Fe_{40}Ni_{40}B_{20}$ MG failure during the tensile test: (a) perpendicular fracture at $T = 300$ K, $\dot{\varepsilon} = 3.3 \times 10^{-6}$ s^{-1}; and (b) oblique fracture at $T = 4.2$ K; $\dot{\varepsilon} = 3.3 \times 10^{-6}$ s^{-1}.

Temperature dependence may be observed also for the difference $\bar{\sigma}_{fr\angle}(T_i) - \bar{\sigma}_{fr\perp}(T_i)$, whose value was 390 MPa at 300 K, 480 MPa for 77 and 640 MPa for 4.2 K. This difference tends to decrease also with increasing deformation rate at 4.2 K, from 790 MPa at $\dot{\varepsilon} = 3.3 \times 10^{-6}$ s^{-1} to 480 MPa at $\dot{\varepsilon} = 1.25 \times 10^{-3}$ s^{-1}.

Most information explaining the existence of two macroscopic failure modes was obtained from the fractographic analysis of the fracture surfaces. On samples failed through a perpendicular fracture it was easy to find the place where the failure initiated, see Fig. 8a, since it was distinguished by an apparent thinning of the sample, sometimes even to "zero" thickness, mostly near ribbon edge. In dependence on temperature and on deformation rate (similarly as in K_c measurements) an area of chevron failure was present near the initiation site on samples failed by such a mode. These samples failed by a mechanism described in [12], where the resulting fracture surface lies alternately in one of two planes forming an angle of approximately 45° with both the ribbon surface and the stress direction [13].

It was more difficult to find the initiation sites on samples which have failed through an oblique fracture, see Fig. 8b. They were always found on the smaller perpendicular part of the fracture surface and they had smaller dimensions that the initiation sites of the perpendicular failure. Only a partial contraction of the ribbon cross section was observed at initiation sites. Larger part of the fracture surface is perpendicular to the ribbon surface and macroscopically makes an angle with the stress axis, whose value locally varies between 25–55°. Vein morphology is observed over the whole width of the fracture surface, only in "corners", where the angle between fracture surface and stress axis locally changes, the traces of shear may be observed, with shear vector parallel to the ribbon surface, Fig. 9.

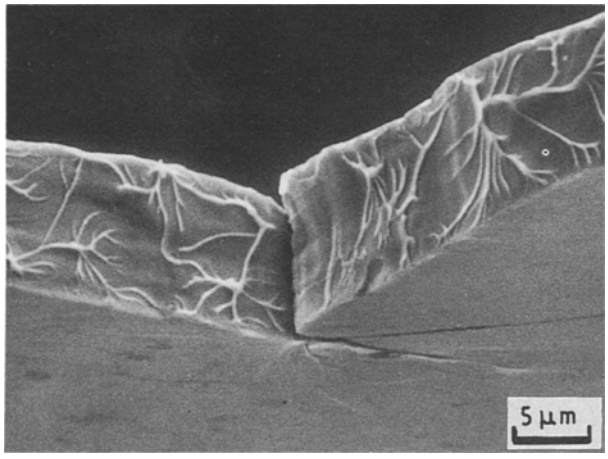

Figure 9 SEM micrograph of the fracture surface of a sample failed through an oblique fracture. Detail from the place where the failure angle changes. It is seen that the vector of the shear displacement is parallel to the ribbon surface.

3. Discussion

It was shown in [5, 6] that the thickness of the amorphous ribbons has an apparent influence on the measured value of K_c and also that the degree of low-temperature embrittlement depends on the degree of the structural relaxation which took place after the preparation of amorphous sample. The thinner the ribbon, the simpler realization of the plane stress conditions, which leads to higher measured values of K_c. Moreover, thinner ribbons are more rapidly cooled during preparation and so their structure needs longer relaxation time to remove the deformation defects facilitating the onset of the inhomogeneous plastic deformation. This explains lower temperatures of embrittlement of the 20 µm thick ribbon we measured as compared with the temperature of embrittlement of the 36 µm thick $Fe_{40}Ni_{40}B_{20}$ ribbon used in [5].

Existence of the non-monotonic $K_c(\dot{\varepsilon})$ dependence at a temperature of 300 K on the $Fe_{40}Ni_{40}B_{20}$ ribbon was put into connection with the dependence of the yield point on the deformation rate [6]. This change of the yield point may be caused by the effects of the mechanical polarization [14] and mechanical annealing [15] of deformation defects in the amorphous structure. The fact, that this dependence was only observed at a temperature of 300 K, indicates that these processes are thermally activated.

From the fractographical point of view it is interesting to note the dependence of the presence of "steps" on smooth parts of the fracture surfaces on the failure temperatures. Presence of these steps indicates a number of closely spaced shear bands, through which the deformation in front of the crack tip was realized. Gradual disappearance of these steps with decreasing temperature gives evidence on the lowering density of potential nuclei for shear bands.

Both macroscopical modes of the MG failure, which we observed, have been already described by Davis [16] as failure at antiplane deformation and failure at general yielding according to von Mises criterion. According to [16], the decisive criterion for which of the two modes of a ductile shear failure will be realized is the relation between the thickness and the width of the amorphous ribbon. However, our fractographical observations and results of fracture stress measurements show that nuclei for both failure modes are represented by defects of the same type, differing only in size and in the degree of ribbon thinning. An important fact expressed by Relation 1 supports the conception that some minimum stress is needed to initiate shear bands at von Mises criterion. But this value of stress is reached only when defect, initiating the failure, is sufficiently small. Therefore the values of $\sigma_{fr\angle}$, which we obtained, do not represent any real yield point, but are only approaching this point from below. A more general criterion for the realization of the one or the other macroscopic failure mode may be found in size and number of regions with lowered cross-sections which are formed during preparation on the contact surface of the quenched ribbon [18]. A statistical distribution of the size of these regions probably exists for particular preparation conditions and, in dependence on the width but also on the length of the tested sample, the existence of the defect with such a size may be expected, which could initiate the perpendicular failure. On the contrary, when due to used technological conditions the distributions of the size of these bubbles is shifted towards lower values, it may be expected, that crack initiation will take place only at stresses at which shear according to von Mises criterion is present. It follows from above said that the realization of any particular failure mode depends on a number of factors: technological influences on the formation of local concentrators on the contact surface of the amorphous ribbon, width and length of the tested samples, but also conditions of the tensile test (temperature and deformation rate) determining the effective size of a concentrator.

The similarity of the $\sigma_{fr\angle}(T,\dot{\varepsilon})$ and $\sigma_{fr\perp}(T,\dot{\varepsilon})$ dependences is clearly seen in Fig. 7. However, the values of $\sigma_{fr\angle}$ for 300 K and 77 K are independent on deformation rate and the following formula is valid in this temperature range

$$(1/\sigma_{fr\angle})\frac{d\sigma_{fr\angle}}{dT} = -5.3\times10^{-4}\,K^{-1} \qquad (3)$$

which correspond to the slope of the Young's modulus of elasticity in this temperature range for $Fe_{40}Ni_{40}B_{20}$ glass [19].

Increase of the percentage of the perpendicular fracture with decreasing temperature is obviously caused by the fact that slowly cooled regions (neighbourhood of surface defects) become brittle sooner at decreasing temperature than the basic amorphous structure [5] and so the effective size of defects increases.

4. Conclusions

Distribution of the defects size on the surface of an amorphous ribbon, dimensions of the tested sample and the conditions of the tensile test (temperature and

deformation rate) are the factors determining what of two modes of the ductile failure will be realized.

The real yield point of the material cannot be determined by a tensile test of wide MG ribbons. Fracture stress of samples, whose larger part did not fail perpendicularly to the stress direction, approaches to the real yield point.

Wiebull character of MG fracture stress distribution is maintained with lowering temperature down to 4.2 K, with simultaneous decrease of the Weibull modulus m.

Existence of the fracture toughness dependence on the deformation rates gives evidence on the presence of thermally activated processes in the amorphous structure which change conditions for the onset of an inhomogeneous plastic deformation in shear bands.

References

1. P. E. DONOVAN and W. M. STOBBS, *Acta Metall.* **29** (1981) 1419.
2. P. G. ZIELINSKI and D. G. AST, *Phil. Mag.* **A48** (1983) 811.
3. R. MADDIN and T. MASUMOTO, *Mat. Sci. Eng.* **9** (1972) 153.
4. V. Z. BENGUS, E. D. TABACHNIKOVA and V. I. STARTSEV, *Phys. Stat. Sol.* **A81** (1984) K11.
5. C. A. PAMPILLO and H. S. CHEN, *Mat. Sci. Eng.* **13** (1974) 181.
6. V. OCELIK, P. DIKO, K. CSACH, V. HAJKO, V. Z. BENGUS, E. D. TABACHNIKOVA, E. B. KOROLKOVA and P. DUHAJ, *J. Mater. Sci.* **22** (1987) 3732.
7. V. OCELIK, V. Z. BENGUS, E. B. KOROLKOVA, E. D. TABACHNIKOVA, K. CSACH and P. DUHAJ, *J. Mater. Sci. Lett.*, **9** (1990) 529.
8. M. CALVO, W. HENNING and F. OSTERSTOCK, in Vth Int. Conf. on RQM, Wurzburg, edited by S. Steeb and H. Warlimont, Proceedings 2 (North-Holland, Amsterdam. 1985) p. 1385.
9. V. OCELIK, P. DIKO, V. HAJKO, J. MISKUF and P. DUHAJ, *J. Mater. Sci.* **22** (1987) 2305.
10. T. K. G. NAMBOODHIRI, T. A. RAMESH, G. SINGH and S. SEHGAL, *Mat. Sci. Eng.* **61** (1983) 23.
11. M. CALVO, *J. Mater. Sci. Lett.* **24** (1989) 1801.
12. F. SPAEPEN and D. TURNBULL, *Scripta Metall.* **8** (1974) 563.
13. V. OCELIK, V. Z. BENGUS, P. DIKO and O. HUDAK, *J. Mater. Sci. Lett.* **6** (1987) 1333.
14. V. Z. BENGUS and V. OCELIK, in XV. International Congress on Glass, Leningrad 2–7. July 1989, edited by O. V. Mazurin, Proceedings 2b, p. 290.
15. D. SROLOVITZ, V. VITEK and T. EGAMI, *Acta Metall.* **31** (1983) 335.
16. L. A. DAVIS, *Scripta Metall.* **9** (1975) 339.
17. C. A. PAMPILLO, *J. Mater. Sci.* **10** (1975) 339.
18. W. A. ELLIOT, F. P. GAGLIANO and G. KRAUSS, *Metall. Trans.* **4A** (1973) 2031.
19. J. C. M. LI, "Ultrarapid Quenching of Liquid Alloys", edited by H. Herman (Academic Press, London, 1981) p. 325.

Received 24 May
and accepted 30 October 1990